SOILS AND FOUNDATIONS Vol. 29, No. 1, 119-137, Mar. 1989
Japanese Society of Soil Mechanics and Fouadation Engineering

AN ISOTROPIC HARDENING ELASTOPLASTIC MODEL FOR SAND CONSIDERING THE STRESS PATH DEPENDENCY IN THREE-DIMENSIONAL STRESSES

TERUO NAKAI[i)]

ABSTRACT

An isotropic hardening elastoplastic constitutive model for sand is developed by extending the model for clay proposed before. This model for sand (named t_{ij}-sand model) can precisely take into consideration the influence of intermediate principal stress on the deformation and strength characteristics by using the concept of the mechanical quantity t_{ij}, and the influence of stress path on the direction of plastic flow by dividing the plastic strain increment into two components, in the same way as the previous model for clay (t_{ij}-clay model). In the present paper, a new "plastic work based on t_{ij}" W^{*p} is defined, and it is experimentally shown that W^{*p} is proper as the quantity of state for sand. Then, the model for sand is formulated by employing W^{*p} as the strain hardening parameter, in place of the plastic volumetric strain ε_v^p in the model for clay.

The validities of the model are confirmed by various shear and consolidation tests under triaxial compression, triaxial extension and three different principal stresse conditions and stress probe tests under triaxial compression and extension conditions. All of the soil parameters of the model can be determined by a conventional triaxial compression test after loading-unloading-reloading isotropic consolidation.

Key words constitutive equation of soil, dilatancy, laboratory test, sand, shear strengh, static, stress path, stress-strain curve (**IGC** : D 6)

INTRODUCTION

When analyzing numerically the behavior of soil foundations and earth structures in practice, we must employ a simple and generalized constitutive model for soils in the analysis ; here, "simple" means not only that the derivation process of model is simple and clear but also that the soil parameters of the model are small in number and can easily be determined, and "generalized" means that the model can uniquely predict various soil behavior under general three-dimensional stress conditions. Now, the well-known

i) Associate Professor, Department of Civil Engineering, Nagoya Institute of Technology, Gokiso-cho, Showa-ku, Nagoya.
Manuscript was received for review on January 27, 1988.
Written discussions on this paper should be submitted before October 1, 1989, to the Japanese Society of Soil Mechanics and Foundation Engineering, Sugayama Bldg. 4 F, Kanda Awaji-cho 2-23, Chiyoda-ku, Tokyo 101, Japan. Upon request the closing date may be extended one month.

Cam-clay model (Roscoe, Schofield and Thurairajah, 1963 ; Schofield and Wroth, 1968), which is one of the simplest models for clay, has problems in the evaluation of the influence of intermediate principal stress, the influence of stress path and others. On the other hand, several more generalized models have recently been developed, but most of them are not simple.

Nakai and Matsuoka (1983 b) developed a constitutive model in which the influence of intermediate principal stress and stress path are properly taken into consideration. In this model, the influence of intermediate principal stress is considered by using the extended concept of "Spatially Mobilized Plane"(briefly SMP*), the influence of stress path by dividing the strain increment into three components (shear, consolidation and elastic components). However, to determine precisely the values of soil parameters of this model, we have to perform two kinds of constant mean principal stress tests under different mean principal stresses and an isotropic consolidation test.

Then, proposed was a simple and generalized elastoplastic constitutive model for clay which is named t_{ij}-clay model (Nakai and Matsuoka, 1986) ; the influence of intermediate principal stress is considered using a mechanical quantity for soil t_{ij} which is the generalized idea of the concept of SMP*, and the influence of stress path is considered by dividing the plastic strain increment into the component satisfying the associated flow rule in t_{ij}-space and the component compressed isotropically, regardless of using one yield function and one strain hardening parameter. As a result, its fundamental soil parameters are the same as those of the Cam-clay model.

In the present study, a simple and generalized elastoplastic model for sand, which is named t_{ij}-sand model, is presented by extending the t_{ij}-clay model mentioned above. On the derivation of this model, we particularly take notice of the following three points where the stress-strain behavior of sand is different from that of clay :

(1) Unlike clay, sand generally shows positive dilatancy in shear even in normally consolidated conditions except for very loose sand.

(2) We usually utilize the concept of state boundarysurface in for mulating models for clay so that plastic volumetric strain $\varepsilon_v{}^p$ is employed as the strain hardening parameter. However, in the case of sand plastic volumetric strain cannot be used as the strain hardening parmeter, since it is not a quantity of state in the same way as the plastic shear strain and others, as mentioned later.

(3) The plastic and elastic volumetric strains of sand under consolidation are accurately given in the form of a power law of mean principal stress p, whereas those of clay are expressed using linear relations between void ratio and ln p.

Throughout this paper, the term "stress" is to be interpreted as "effective stress".

DEFINITION OF MECHANICAL QUANTITY t_{ij} AND STRESS AND PLASTIC STRAIN INCREMENT PARAMETERS USED

In most of elastoplastic constitutive models such as the Cam-clay model, the yield function and/or the plastic potential functions are formulated using the following stress parameters and plastic strain increment parameters

$$p=\frac{1}{2}(\sigma_1+\sigma_2+\sigma_3)=\frac{1}{3}\sigma_{ii} \tag{1}$$

$$q=\frac{1}{\sqrt{2}}\sqrt{(\sigma_1-\sigma_2)^2+(\sigma_2-\sigma_3)^2+(\sigma_3-\sigma_1)^2}$$
$$=\sqrt{(\sigma_{ii})^2-(3/2)\sigma_{ij}\sigma_{ij}} \tag{2}$$

$$d\varepsilon_v{}^p=d\varepsilon_1{}^p+d\varepsilon_2{}^p+d\varepsilon_3{}^p=d\varepsilon_{ii}{}^p \tag{3}$$

$$d\varepsilon_d{}^p=\frac{\sqrt{2}}{3}\sqrt{\begin{array}{l}(d\varepsilon_1{}^p-d\varepsilon_2{}^p)^2+(d\varepsilon_2{}^p\\ -d\varepsilon_3{}^p)^2+(d\varepsilon_3{}^p-d\varepsilon_1{}^p)^2\end{array}}$$
$$=\frac{2}{3}\sqrt{(d\varepsilon_{ii}{}^p)^2-(3/2)d\varepsilon_{ij}{}^p d\varepsilon_{ij}{}^p} \tag{4}$$

However, it has been known that constitutive models using these parameters cannot describe the stress-strain behavior of soil in three-dimensional stresses uniquely. Then, a mechanical quantity t_{ij} has been proposed

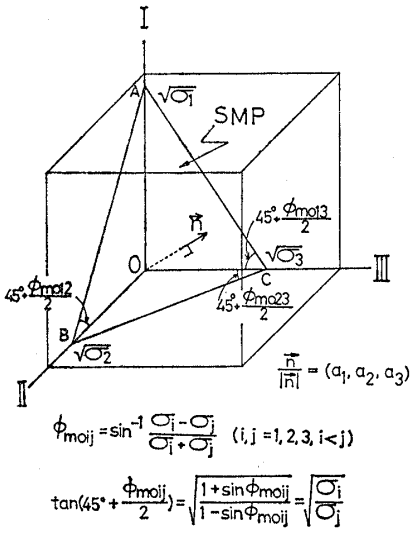

Fig. 1. A cubical soil element and Spatially Mobilized Plane (plane *ABC*) in three-dimensional stresses

to describe the three-dimensional stress-strain behavior of soils, and an elastoplastic model for clay using this t_{ij}-concept has been developed. Since the details of this mechanical quantity t_{ij} and the model for clay are described in other papers (Nakai and Mihara, 1984 ; Nakai and Matsuoka, 1986), we will show here only the outline of the concept of t_{ij}.

Fig. 1 shows a cubical soil element and the "Spatially Mobilized plane (SMP)" in a three-dimensional space, where I, II and III axes represent the directions to which three principal stresses σ_1, σ_2 and σ_3 are applied, respectively. The SMP is the plane ABC, and the values at the points (A, B and C) where the SMP intersects these three axes are proportional to the square roots of the respective principal stresses (Matsuoka and Nakai, 1974, 1977). The direction cosines (a_1, a_2 and a_3) of the normal to the SMP are expressed as

$$a_i=\sqrt{\frac{J_3}{\sigma_i J_2}} \quad (i=1,2,3) \qquad (5)$$

where J_1, J_2 and J_3 are the first, second and third effective stress invariants and expressed by the following forms using three principal stresses :

$$\left.\begin{aligned} J_1&=\sigma_2+\sigma_2+\sigma_3 \\ J_2&=\sigma_1\sigma_2+\sigma_2\sigma_3+\sigma_3\sigma_1 \\ J_3&=\sigma_1\sigma_2\sigma_3 \end{aligned}\right\} \qquad (6)$$

The mechanical quantity t_{ij} is given by the following tensor which is expressed by the product of stress tensor σ_{ik} and tensor a_{kj} which has principal values of (a_1, a_2 and a_3).

$$t_{ij}=\sigma_{ik}a_{kj} \qquad (7)$$

Here, t_{ij} is a symmetric tensor whose principal directions coincide with those of σ_{ij}, because both σ_{ij} and a_{ij} are symmetric tensors and the principal directions of σ_{ij} and a_{ij} coincide. The tensor a_{ij} is concretely given by the following equation.

$$a_{ij}=\sqrt{J_3/J_2}\cdot(\sigma_{ik}+I_2\cdot\delta_{ik})(I_1\cdot\sigma_{kj}+I_3\cdot\delta_{kj})^{-1} \qquad (8)$$

The derivation process of Eq. (8) and the definition of (I_1, I_2 *and* I_3) are indicated in Appendix I.

The stress parameters (t_N and t_S) used in the model based on the t_{ij}-concept are given by the normal component ON and the parallel component NT of the principal value vector of t_{ij}, $\overrightarrow{OT}=\vec{t}_i=(t_1,\ t_2,\ t_3)$, to the SMP as shown in Fig. 2, and are also equivalent to the normal and shear stresses (σ_{SMP} and τ_{SMP}) on the SMP, respectively.

$$t_N=t_1a_1+t_2a_2+t_3a_3=t_{ij}a_{ij} \qquad (9)_1$$

$$\left(\equiv\sigma_{SMP}=\sigma_1a_1^2+\sigma_2a_2^2+\sigma_3a_3^2=3\frac{J_3}{J_2}\right) \qquad (9)_2$$

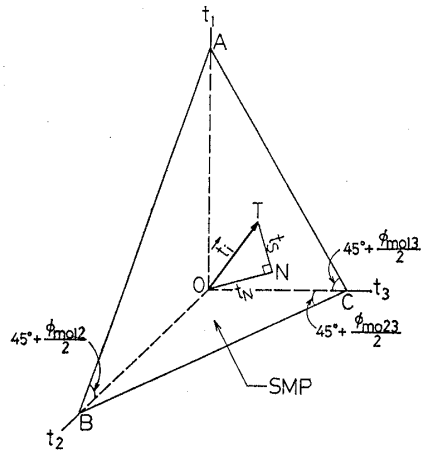

Fig. 2. Stress parameters (t_N and t_S) represented in principal value space of t_{ij}

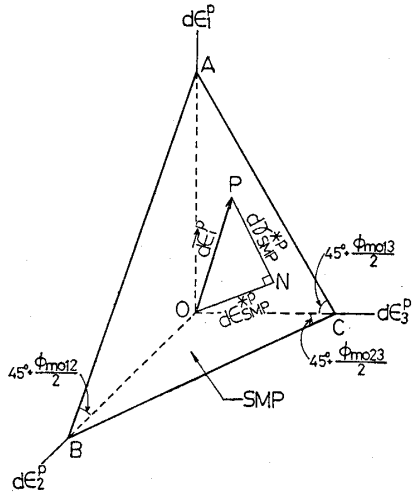

Fig. 3. Plastic strain increment parameters ($d\varepsilon_{SMP}{}^{*p}$ and $d\gamma_{SMP}{}^{*p}$) represented in plastic principal strain increment space

$$t_S=\sqrt{(t_1{}^2+t_2{}^2+t_3{}^2)-t_N{}^2}$$
$$=\sqrt{t_{ij}t_{ij}-(t_{ij}a_{ij})^2} \qquad (10)_1$$
$$\left(\equiv\tau_{SMP}=\sqrt{\begin{array}{r}(\sigma_1-\sigma_2)^2a_1{}^2a_2{}^2+(\sigma_2-\sigma_3)^2a_2{}^2a_3{}^2\\+(\sigma_3-\sigma_1)^2a_3{}^2a_1{}^2\end{array}}\right.$$
$$\left.=\frac{\sqrt{J_1J_2J_3-9J_3{}^2}}{J_2}\right) \qquad (10)_2$$

Similarly, if it is assumed that the directions of plastic principal strain increments coincide with those of principal axes of t_{ij}, the plastic strain increment parameters ($d\varepsilon_{SMP}{}^{*p}$ and $d\gamma_{SMP}{}^{*p}$) are also given by the normal component ON and parallel component NP of the plastic principal strain increment vector, $\overrightarrow{OP}=\overrightarrow{d\varepsilon_i{}^p}=(d\varepsilon_1{}^p,\ d\varepsilon_2{}^p,\ d\varepsilon_3{}^p)$, to the SMP as shown in Fig. 3.

$$d\varepsilon_{SMP}{}^{*p}=d\varepsilon_1{}^pa_1+d\varepsilon_2{}^pa_2+d\varepsilon_3{}^pa_3$$
$$=d\varepsilon_{ij}{}^pa_{ij} \qquad (11)$$
$$d\gamma_{SMP}{}^{*p}=\sqrt{(d\varepsilon_1{}^{p2}+d\varepsilon_2{}^{p2}+d\varepsilon_3{}^{p2})-d\varepsilon_{SMP}{}^{*p2}}$$
$$=\sqrt{d\varepsilon_{ij}{}^pd\varepsilon_{ij}{}^p-(d\varepsilon_{ij}{}^pa_{ij})^2} \qquad (12)$$

According to the t_{ij}-concept, if we make a yield function and/or a plastic potential function using the stress parameter (t_N and t_S) given by Eqs. (9) and (10) instead of (p and q) given by Eqs. (1) and (2) and assume the flow rule in t_{ij}-space instead of σ_{ij}-space, the stress-strain behavior in three-dimensional stresses can be described with unified soil parameters.

QUANTITY OF STATE FOR SAND

In elastoplastic constitutive models for clay based on the critical state concept (e. g. Schofield and Wroth, 1968 ; Roscoe and Burland, 1968), plastic volumetric strain, $\varepsilon_v{}^p$, (or void ratio e) is used as the strain hardening parameter, because it has experimentally been confirmed that void ratio of clay is a quantity of state which is determined by the current stress condition alone regardless of the stress path history (Henkel, 1960). On the other hand, it has been indicated that void ratio is not necessarily a quantity of state for sand (Tatsuoka, 1972). Then, in this section we will discuss about the quantity of state for sand on the basis of triaxial compression and extension test results.

Fig. 4 shows the stress paths in triaxial tests on medium dense Toyoura sand (initial void ratio $e_0\simeq 0.68$) in terms of the relation between axial stress σ_a and radial stress σ_r. Here, points A, B and C represent the isotropic stress conditions ($R\equiv\sigma_1/\sigma_3=1$) where respective mean principal stresses p are 196, 392 and 588 kN/m² ; points D, E, F and G the anisotropic stress conditions ($R\equiv$

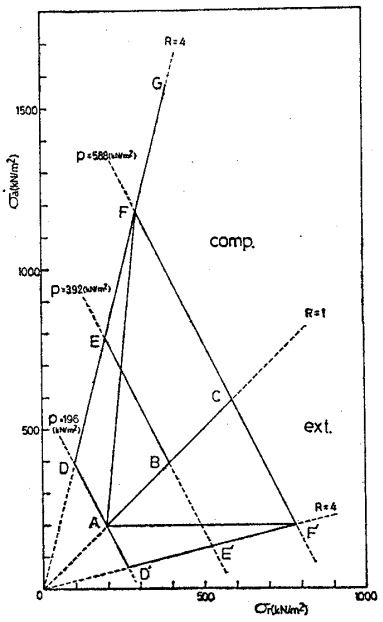

Fig. 4. Stress paths of triaxial compression and extension tests for examining quantity of state for sand

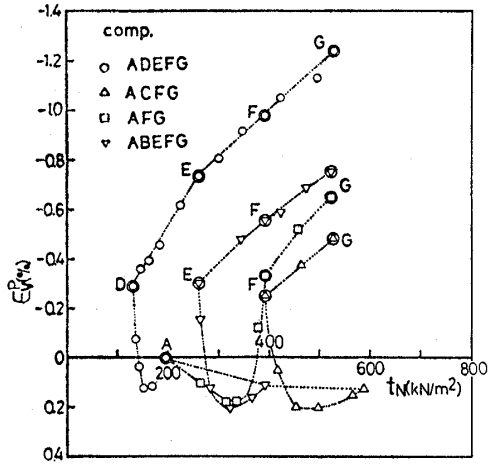

(a) triaxial compression

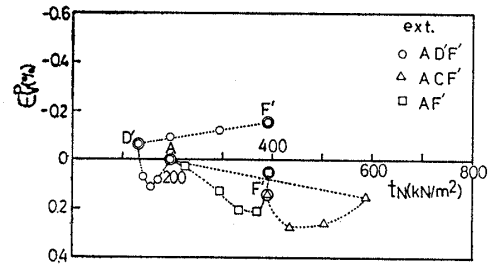

(b) triaxial extension

Fig. 5. Relation between ε_v^p and t_N

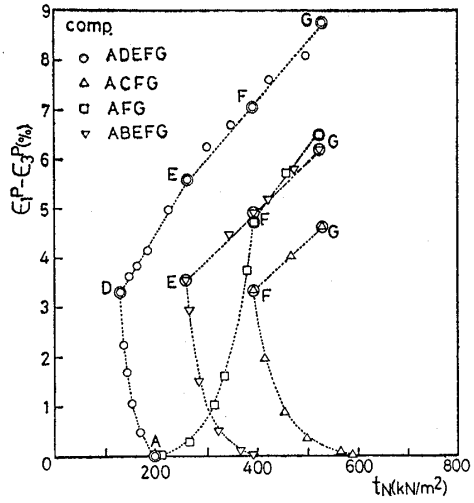

(a) triaxial compression

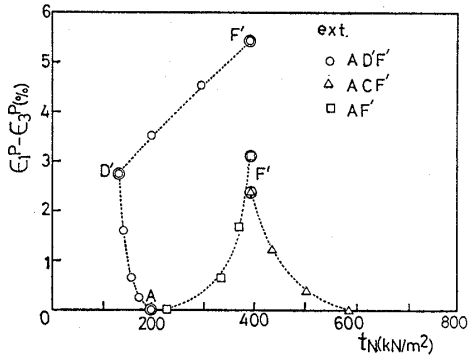

(b) triaxial extension

Fig. 6. Relation between $(\varepsilon_1^p-\varepsilon_3^p)$ and t_N

$\sigma_1/\sigma_3=\sigma_a/\sigma_r=4$) in triaxial compression; points D′, E′ and F′ the anisotropic stress conditions ($R\equiv\sigma_1/\sigma_3=\sigma_r/\sigma_a=4$) in triaxial extension. Performing four kinds of triaxial compression tests (paths : *ADEFG*, *ACFG*, *AFG* and *ABEFG*) and three kinds of triaxial extension tests (paths : *AD′F′*, *AC′F′* and *AF′*), we will discuss what physical quantity is appropriate as the quantity of state for sand. Let us consider four quantities—the plastic volumetric strain ε_v^p, the plastic principal strain difference $\varepsilon_1^p-\varepsilon_3^p$, the plastic work $W^p=\int\sigma_{ij}d\varepsilon_{ij}^p$ and the "plastic work based on t_{ij}" W^{*p} which is given by

$$W^{*p}=\int t_{ij}d\varepsilon_{ij}^p$$
$$=\int(t_N\cdot d\varepsilon_{SMP}^{*p}+t_S\cdot d\gamma_{SMP}^{*p}) \qquad (13)$$

where t_{ij} is the mechanical quantity given by Eq. (7), and (t_N and t_S) and ($d\varepsilon_{SMP}^{*p}$ and $d\gamma_{SMP}^{*p}$) are the stress parameters and the plastic strain increment parameters given by Eqs. (9) to (12), respectively. The validity of second equal sign in Eq. (13) is discussed in Appendix II. Figs. 5 to 8 show the variations in these quantities along the seven kinds of stress paths under triaxial compression and extension conditions. In these figures, the axes of abscissas represent the values of t_N which is given by the following equation using mean principal stress p and stress ratio $X\equiv t_S/t_N$.

$$t_N=\frac{p}{X^2+1} \qquad (14)$$

The dots enclosed with circle in these figures denote the observed values at the stress conditions of A, D, E, F, G, D′ and F′. It is obvious from Figs. 5 and 6 that the plastic volumetric strain ε_v^p used in most of constitutive models for clay and the plastic principal strain difference $\varepsilon_1^p-\varepsilon_3^p$ (or the plastic octahedral shear strain γ_{oct}^p) are unsuitable to

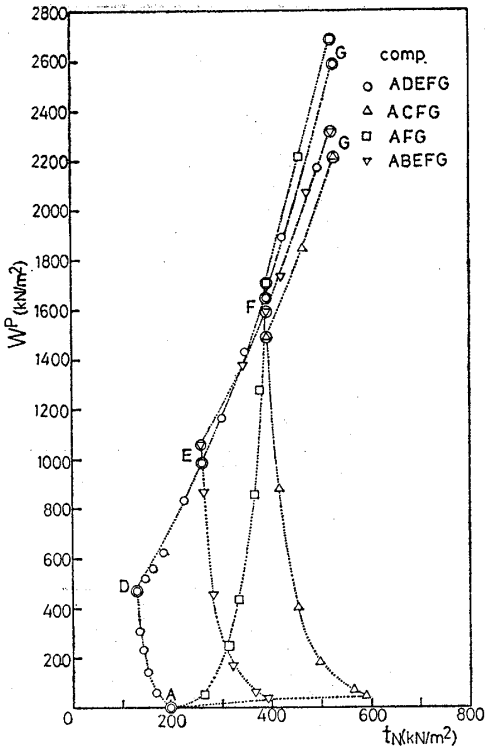

(a) triaxial compression

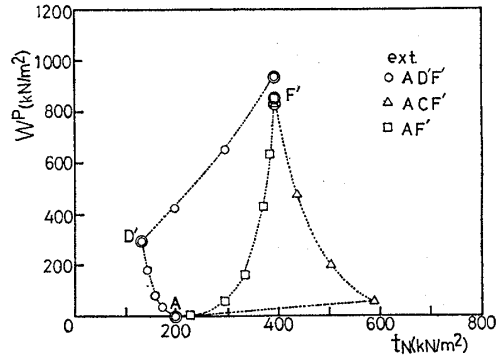

(b) triaxial extension

Fig. 7. Relation between W^p and t_N

the quantity of state for sand, because these plastic strains depend on the stress paths at the same stress state. Next, as is seen from Fig. 7, the plastic work W^p does not much depend on the stress paths if the stress conditions are limited in triaxial compression or triaxial extension alone. However, from the comparison between diagrams (a) and (b), we can find that the values of W^p in triaxial compression are larger than those in triaxial extension at the same stress ratio and mean stresses(for example, compare the values at D and F with those at D′ and F′, respectively). Thus, W^p also may be inappropriate as the strain hardening parameter of the constitutive model for sand in three-dimensional stresses. On the other hand, Fig. 8 may indicate that the values of "plastic work based on t_{ij}" W^{*p} are uniquely determined regardless of the stress path history and the stress conditions (e. q. difference between triaxial compression and extension). We therefore employ "plastic work based on t_{ij}" W^{*p} as a strain hardening parameter of the present model for sand.

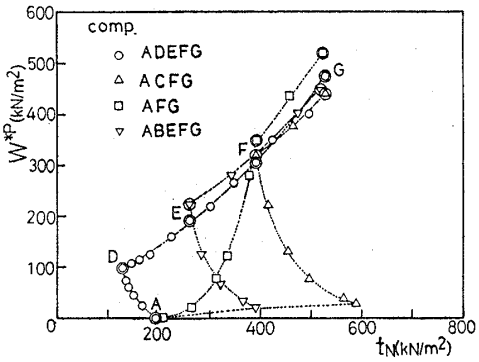

(a) triaxial compression

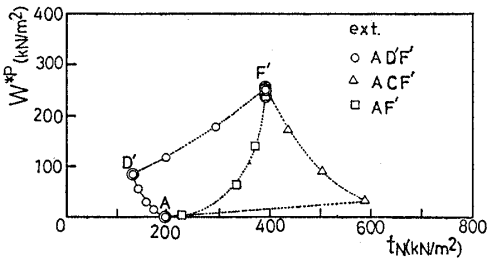

(b) triaxial extension

Fig. 8. Relation between W^{*p} and t_N

ELASTOPLASTIC CONSTITUTIVE MODEL FOR SAND

The plastic strain increment tensor $d\varepsilon_{ij}^p$ is assumed to be divided into two components : the plastic strain increment which satisfies the associated flow rule in the t_{ij}-space, $d\varepsilon_{ij}^{p(AF)}$, and the plastic strain increment compressive isotropically, $d\varepsilon_{ij}^{p(IC)}$, in the same manner as the model for clay proposed previously (Nakai and Matsuoka, 1986).

$$d\varepsilon_{ij}^p = d\varepsilon_{ij}^{p(AF)} + d\varepsilon_{ij}^{p(IC)} \qquad (15)$$

These two components are given by the following equations, because the direction of $d\varepsilon_{ij}^{p(AF)}$ is normal to the yield surface f in the t_{ij}-space, and $d\varepsilon_{ij}^{p(IC)}$ is the isotropic strain increment :

$$d\varepsilon_{ij}^{p(AF)}=\Lambda\cdot\frac{\partial f}{\partial t_{ij}} \tag{16}$$

$$d\varepsilon_{ij}^{p(IC)}=K\langle dp\rangle\cdot\frac{\delta_{ij}}{3}\quad(p=\sigma_{ii}/3) \tag{17}$$

Here, δ_{ij} is the Kronecker delta, and $\langle dp\rangle$ implies that

$$\langle dp\rangle=\begin{cases}dp & \text{if } dp>0\\ 0 & \text{if } dp\leqq 0\end{cases} \tag{18}$$

Throughout this paper, superscripts e, p, (AF) and (IC) denote the elastic component, the plastic component, the component satisfying the associated flow rule and the component compressive isotropically, respectively.

Determination of $d\varepsilon_{ij}^{p(IC)}$

It is well known that there are linear relationships between elastic and plastic volumetric strains (ε_v^e and ε_v^p) and ln p (p= mean principal stress) in the consolidation test on clay. On the other hand, in the case of sand these volumetric strains under isotropic consolidation are exactly expressed not by the linear relationships to the logarithm of mean stress but by the following power law of mean stress

$$\varepsilon_v^e=C_e\left\{\left(\frac{p}{P_a}\right)^m-\left(\frac{p_0}{P_a}\right)^m\right\} \tag{19}$$

$$\varepsilon_v^p=(C_t-C_e)\left\{\left(\frac{p}{P_a}\right)^m-\left(\frac{p_0}{P_a}\right)^m\right\} \tag{20}$$

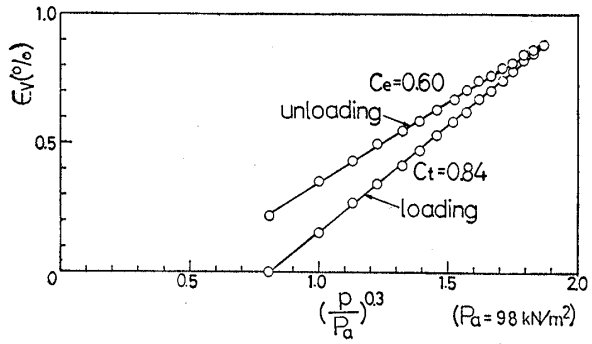

Fig. 9. Results of loading and unloading isotropic consolidation tests on Toyoura sand

where p_0 is the initial mean principal stress and P_a (=98 kN/m²) is the atmospheric pressure. Fig. 9 shows the results of the loading and unloading isotropic consolidation tests on medium dense Toyoura sand ($e_0\simeq 0.68$), as plotted in terms of the relation between ε_v and $(p/P_a)^m$. From this figure, the coefficients in Eqs. (19) and (20) for Toyoura sand are determined as $C_t=0.84$, $C_e=0.60$ and $m=0.3$ for dense sand. If it is assumed that plastic volumetric strain compressive isotropically is given by Eq. (20) regardless of stress state, $d\varepsilon_{ij}^{p(IC)}$ of Eq. (17) are expressed as

$$\begin{aligned}d\varepsilon_{ij}^{p(IC)}&=d\varepsilon_v^{p(IC)}\cdot\frac{\delta_{ij}}{3}\\&=m(C_t-C_e)\frac{p^{m-1}}{P_a{}^m}\langle dp\rangle\frac{\delta_{ij}}{3}\\&=K\langle dp\rangle\frac{\delta_{ij}}{3}\end{aligned} \tag{21}$$

so that the coefficient K in Eq. (17) is

$$K=m(C_t-C_e)\frac{p^{m-1}}{P_a{}^m} \tag{22}$$

Determination of $d\varepsilon_{ij}^{p(AF)}$

It can be considered that there is the following unique relation between the stress ratio (t_S/t_N) and the plastic strain increment ratio ($d\varepsilon_{SMP}{}^{*p(AF)}/d\gamma_{SMP}{}^{*p(AF)}$) in the same way as the t_{ij}-clay model :

$$Y=\frac{X_f-X}{\alpha}+Y_f \tag{23}$$

in which $X\equiv t_S/t_N$, $Y\equiv d\varepsilon_{SMP}{}^{*p(AF)}/d\gamma_{SMP}{}^{*p(AF)}$,

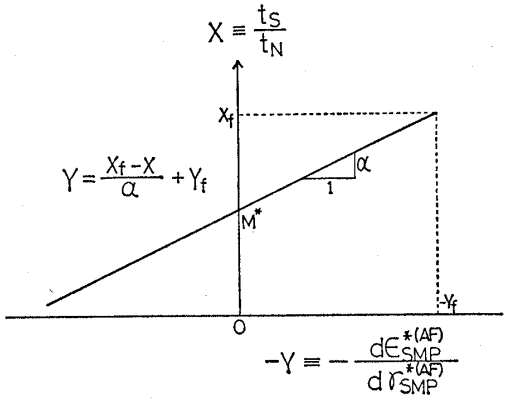

Fig. 10. Proposed relation between stress ratio (t_S/t_N) and plastic strain increment ratio ($-d\varepsilon_{SMP}{}^{*p(AF)}/d\gamma_{SMP}{}^{*p(AF)}$)

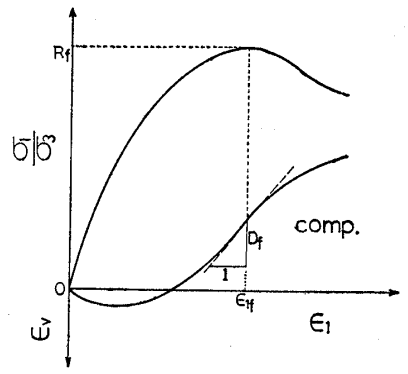

Fig. 11. Explanation of R_f and D_f

and X_f and Y_f are the values of X and Y at failure (see Fig. 10). Now, X_f and Y_f are determined as follows using the principal stress ratio at failure, R_f, and the gradient of dilatancy curve at failure, D_f, in a conventional triaxial compression test as shown in Fig. 11 : if it is considered that the strength of soils in three-dimensional stresses is uniquely described by the SMP failure criterion (Matsuoka and Nakai, 1974, 1977), X_f is expressed in terms of R_f from Eqs. (9) and (10) and the condition of $\sigma_2=\sigma_3$ and $a_2=a_3$.

$$X_f\equiv(t_S/t_N)_f\equiv(\tau_{SMP}/\sigma_{SMP})_f =\frac{\sqrt{2}}{3}\left(\sqrt{R_f}-\sqrt{\frac{1}{R_f}}\right) \tag{24}$$

Furthermore, under the triaxial compression condition ($\sigma_1>\sigma_2=\sigma_3$ and $d\varepsilon_1>d\varepsilon_2=d\varepsilon_3$) the plastic strain increment ratio Y is expressed in the following form from Eqs. (11)and (12).

$$Y\equiv\frac{d\varepsilon_{SMP}{}^{*p}}{d\gamma_{SMP}{}^{*p}}=\frac{d\varepsilon_1{}^p a_1+2d\varepsilon_3{}^p a_3}{\sqrt{2}\,(d\varepsilon_1{}^p a_3-d\varepsilon_3{}^p a_1)} =\frac{1+2\sqrt{\dfrac{\sigma_1}{\sigma_3}}\cdot\left(\dfrac{d\varepsilon_3{}^p}{d\varepsilon_1{}^p}\right)}{\sqrt{2}\left\{\sqrt{\dfrac{\sigma_1}{\sigma_3}}-\left(\dfrac{d\varepsilon_3{}^p}{d\varepsilon_1{}^p}\right)\right\}} \tag{25}$$

Here, since at failure the elastic strain increment becomes relatively small in comparison with the plastic strain increment and the strain increment ratio is hardly affected by the stress paths, the plastic strain increment ratio at failure Y_f is given using R_f and D_f in a conventional triaxial compression test.

$$Y_f=\frac{1+2\sqrt{R_f}\cdot\left\{\dfrac{1}{2}\left(\dfrac{d\varepsilon_v{}^p}{d\varepsilon_1{}^p}\right)_f-\dfrac{1}{2}\right\}}{\sqrt{2}\left\{\sqrt{R_f}-\dfrac{1}{2}\left(\dfrac{d\varepsilon_v{}^p}{d\varepsilon_1{}^p}\right)_f+\dfrac{1}{2}\right\}} =\frac{1-\sqrt{R_f}(1-D_f)}{\sqrt{2}\,\{R_f+0.5(1-D_f)\}} \tag{26}$$

where

$$R_f\equiv\left(\frac{\sigma_1}{\sigma_3}\right)_{f(\text{comp.})}=\frac{1+\sin\phi'_{(\text{comp.})}}{1-\sin\phi'_{(\text{comp.})}} \tag{27}$$

and

$$D_f\equiv\left(\frac{d\varepsilon_v}{d\varepsilon_1}\right)_{f(\text{comp.})} \tag{28}$$

Throughout this paper, symbols with subscripts f, (comp.) and (ext.) denote the values at failure, under triaxial compression condition and under triaxial extension condition, respectively.

Because it is assumed that the directions of principal axes of t_{ij} coincide with those of the plastic principal strain increments and the associated flow rule holds in the t_{ij}-space, the following normality condition can be obtained.

$$dt_{ij}d\varepsilon_{ij}{}^{p(AF)}=dt_N\cdot d\varepsilon_{SMP}{}^{*p(AF)} +dt_S\cdot d\gamma_{SMP}{}^{*p(AF)}=0 \tag{29}$$

Solving the differential equation which is derived by combining Eqs. (23) and (29) gives

$$\ln t_N+\frac{-\alpha}{1-\alpha}\ln\left|1-(1-\alpha)\frac{X}{M^*}\right|-\ln t_{N1}=0 \tag{30}$$

where M^* is the ordinate intercept in Fig. 10 and given by

$$M^*=X_f+\alpha Y_f \tag{31}$$

and t_{N1} is the value of t_N at $t_S=0$.

Now, as mentioned in a previous section, we employ the "plastic work based on t_{ij}", W^{*p}, given by Eq. (13) as a hardening parameter (Nakai, 1987). Under the virgin isotropic consolidation ($\sigma_1=\sigma_2=\sigma_3$), t_N, t_S, $d\varepsilon_{SMP}{}^{*p}$ and $d\gamma_{SMP}{}^{*p}$ given by Eqs. (9) to (12) are expressed in the following form because $a_1=a_2=a_3=1/\sqrt{3}$ and $d\varepsilon_1{}^p=d\varepsilon_2{}^p=d\varepsilon_3{}^p$

$$t_N=p \tag{32}$$

$$t_S=0 \tag{33}$$

$$d\varepsilon_{SMP}{}^{*p}=\frac{d\varepsilon_v{}^p}{\sqrt{3}}=\frac{m(C_t-C_e)}{\sqrt{3}\,P_a{}^m}p^{m-1}\cdot dp$$
$$=\frac{m(C_t-C_e)}{\sqrt{3}\,P_a{}^m}t_N{}^{m-1}\cdot dt_N \qquad (34)$$
$$d\gamma_{SMP}{}^{*p}=0 \qquad (35)$$

where Eq. (20) is utilized to obtain Eq. (34). Therefore, when the stress condition (t_N, t_S) changes from (t_{N0}, 0) to (t_{N1}, 0), Eq. (13) defining W^{*p} takes the form

$$W^{*p}=\int t_N d\varepsilon_{SMP}{}^{*p}$$
$$=\int_{t_{N0}}^{t_{N1}}\frac{m(C_t-C_e)}{\sqrt{3}\,P_a{}^m}t_N{}^m dt_N$$
$$=K_1\cdot\{t_{N1}{}^{m+1}-t_{N0}{}^{m+1}\} \qquad (36)$$

where

$$K_1=\frac{m(C_t-C_e)}{\sqrt{3}\,(m+1)P_a{}^m} \qquad (37)$$

From Eq. (36), t_{N1} is expressed as

$$t_{N1}=\left(\frac{W^{*p}}{K_1}+t_{N0}{}^{m+1}\right)^{1/m+1} \qquad (38)$$

Substituting Eq. (38) into Eq. (30), we can obtain the following yield function because the direction of $d\varepsilon_{ij}{}^{p(AF)}$ is normal to the yield function

$$f=\ln t_N+\frac{-\alpha}{1-\alpha}\ln\left|1-(1-\alpha)\frac{X}{M^*}\right|$$
$$-\frac{1}{m+1}\ln\left(\frac{W^{*p}}{K_1}+t_{N0}{}^{m+1}\right)=0 \qquad (39)$$
($W^{*p}=0$ when $t_N=t_{N0}$ and $t_S=0$)

Now that the yield function is given by the above equation, we can calculate $d\varepsilon_{ij}{}^{p(AF)}$ using Eq. (16). Here, the proportionality constant Λ in Eq. (16) is determined as follows: since the yield function f is given in the form of $f=f(t_{ij}, a_k, W^{*p})=f(\sigma_{ij}, W^{*p})=0$, the consistency condition reads

$$\frac{\partial f}{\partial\sigma_{ij}}d\sigma_{ij}+\frac{\partial f}{\partial W^{*p}}dW^{*p}=0 \qquad (40)$$

The increment dW^{*p} is given in the following form by using Eqs. (15) to (17)

$$dW^{*p}=t_{ij}d\varepsilon_{ij}{}^p=t_{ij}(d\varepsilon_{ij}{}^{p(AF)}+d\varepsilon_{ij}{}^{p(IC)})$$
$$=t_{ij}\left(\Lambda\frac{\partial f}{\partial t_{ij}}+K\langle dp\rangle\frac{\delta_{ij}}{3}\right) \qquad (41)$$

Combining Eqs. (40) and (41), we determine Λ in the form.

$$\Lambda=-\frac{\frac{\partial f}{\partial\sigma_{ij}}d\sigma_{ij}+\frac{\partial f}{\partial W^{*p}}t_{mn}\frac{\delta_{mn}}{3}K\langle dp\rangle}{\frac{\partial f}{\partial W^{*p}}\frac{\partial f}{\partial t_{kl}}t_{kl}} \qquad (42)$$

where from Eq. (39), $\partial f/\partial W^{*p}$ is expressed as

$$\frac{\partial f}{\partial W^{*p}}=\frac{-1}{(m+1)(W^{*p}+K_1t_{N0}{}^{m+1})} \qquad (43)$$

Complete Form of the Constitutive Model

The elastic strain increment tensor $d\varepsilon_{ij}{}^e$ is given by use of generalized Hooke's law

$$d\varepsilon_{ij}{}^e=\frac{1+\nu}{E_e}d\sigma_{ij}-\frac{\nu_e}{E_e}d\sigma_{kk}\delta_{ij} \qquad (44)$$

where Young's modulus E_e can be expressed as follows by utilizing that $d\varepsilon_{ii}{}^e=d\varepsilon_v{}^e$ satisfies Eq. (19).

$$E_e=\frac{3(1-2\nu_e)P_a{}^m}{mC_e p^{m-1}}$$
(ν_e=Poisson's ratio) (45)

Therefore, the total strain increment tensor $d\varepsilon_{ij}$ is given by the following form as the summation of $d\varepsilon_{ij}{}^p$ in Eqs. (15) to (17) and $d\varepsilon_{ij}{}^e$ in Eq. (44).

$$d\varepsilon_{ij}=d\varepsilon_{ij}{}^p+d\varepsilon_{ij}{}^e$$
$$=d\varepsilon_{ij}{}^{p(AF)}+d\varepsilon_{ij}{}^{p(IC)}+d\varepsilon_{ij}{}^e \qquad (46)$$

Here, $d\varepsilon_{ij}{}^{p(AF)}$ is calculated from Eqs. (16), (39) and (42), $d\varepsilon_{ij}{}^{p(IC)}$ from Eqs. (17) and (22), and $d\varepsilon_{ij}{}^e$ from Eqs. (44) and (45).

Let us summarize the development of strains under various stress paths using Fig. 12 where the yield surface ($f=0$) is drawn in the (t_N, t_S) space.

(i) If the stress condition lies inside the current yield surface or moves from point A to region I ($f<0$ or $df\leqq 0$):

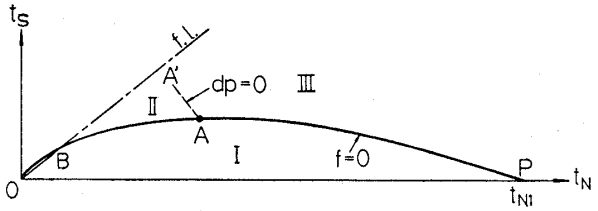

Fig. 12. Proposed yield surface f represented in (t_N, t_S) space and three regions where developments of strain are different when stress condition moves from point A

$$d\varepsilon_{ij}=d\varepsilon_{ij}{}^{e} \tag{47}$$

(ii) If the stress condition moves from point A to region II ($f=0$, $df>0$ and $dp\leqq 0$) :

$$d\varepsilon_{ij}=d\varepsilon_{ij}{}^{p(AF)}+d\varepsilon_{ij}{}^{e} \tag{48}$$

(iii) If the stress condition moves from point A to region III ($f=0$, $df>0$ and $dp>0$) :

$$d\varepsilon_{ij}=d\varepsilon_{ij}{}^{p(AF)}+d\varepsilon_{ij}{}^{p(IC)}+d\varepsilon_{ij}{}^{e} \tag{49}$$

VERIFICATION OF PROPOSED MODEL

Sand Used and Determination of Its Soil Parameters

Saturated Toyoura sand was used in the experiments. The mean diameter of the sand is 0.2 mm, the uniformity coefficient is 1.3 and the specific gravity is 2.65. The maximum and minimum void ratios of the sand are 0.95 and 0.58. Each of the specimen was prepared not to have inherent anisotropic structure, and to be medium dense (initial void ratio $e_0\simeq 0.68$). The details of specimens, apparatus and test procedure was described in a former paper (Nakai and Matsuoka, 1983 a). Some of the test results presented in this paper also are the same as those reported in the former paper.

The values of soil parameters of the medium dense Toyoura sand ($e_0\simeq 0.68$) are listed in Table 1. The values of (C_t, C_e and m) are determined from a loading and unloading isotropic consolidation test, since the plastic and elastic volumetric strains, $\varepsilon_v{}^{e}$ and $\varepsilon_v{}^{p(IC)}$, are given by Eqs. (19) snd (20), respectively (see Fig. 9). Next, R_f and D_f, which stand for the principal stress ratio $(\sigma_1/\sigma_3)_f$ and the strain increment ratio $(d\varepsilon_v/d\varepsilon_1)_f$ at failure under triaxial compression, are determined from an arbitrary drained triaxial compression test (see Fig. 11). This is because the stress ratio and the strain increment ratio of sand at failure are independent of the change in mean stress under shear loading. Lastly, while α denotes the linear gradient in Fig. 10, it is not necessary that the value is determined from such an arrangement shown in this figure. Since the value of α usually lies between 0.6 and 0.9, we can estimate the value of α by assuming a proper value of α and fitting the calculated stress-strain curve to a test result : e.g. the above-mentioned triaxial compression test which is utilized to determine R_f and D_f. Generally, the value of Poisson's ratio of elastic materials is not less than 0.0. So, the value of Poisson's ratio ν_e in Eqs. (44) and (45) is usually assumed to be 0.0, because the elastic shear strain of sands is relatively small.

Table 1. Values of soil parametere for Toyoura sand used in analysis

C_t	0.84×10^{-2}
C_e	0.60×10^{-2}
m	0.3
$R_f\equiv(\sigma_1/\sigma_3)_{f(\mathrm{comp.})}$	4.7
$D_f\equiv(d\varepsilon_v/d\varepsilon_1)_{f(\mathrm{comp.})}$	−0.6
α	0.85

Consequently, all of the soil parameters can be determined by performing a conventional triaxial compression test (e.g. constant radial stress test) after loading-unloading-reloading isotropic consolidation, as shown in Fig. 13.

Consideration of Stress Ratio-Strain Increment Ratio Relationships

Fig. 14 shows results of various triaxial compression and extension tests (p=const., σ_3=const., σ_1=const. and $R\equiv\sigma_1/\sigma_3$=const.) with respect to the relation between the stress

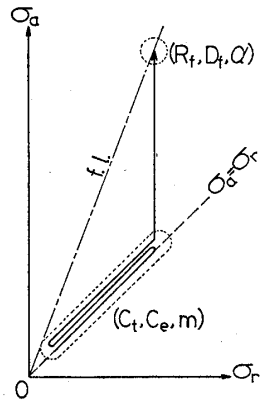

Fig. 13. Stress path of test to determine values of soil parameters

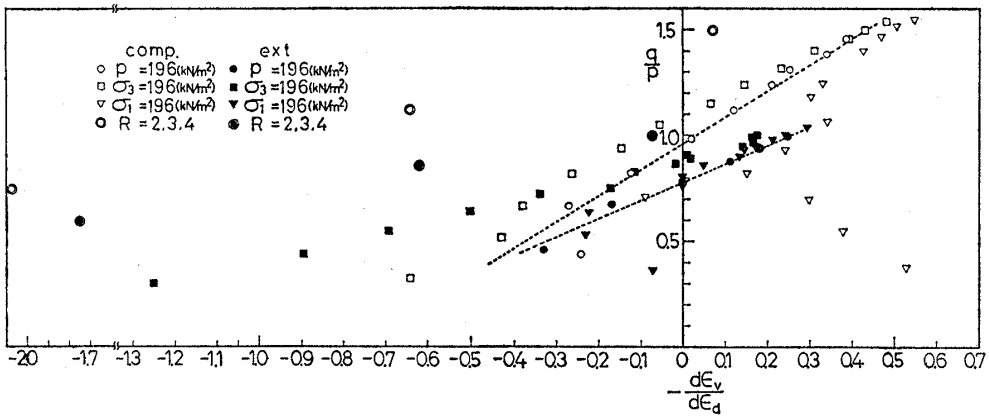

Fig. 14. Relation between q/p and $d\varepsilon_v/d\varepsilon_d$ in triaxial compression and extension tests under various stress paths

ratio q/p and strain increment ratio $d\varepsilon_v/d\varepsilon_d$, according to the stress and strain increment parameters used in most of the models such as Cam-clay model. Fig. 15 also shows the same results in terms of the relation t_S/t_N and $d\varepsilon_{SMP}{}^*/d\gamma_{SMP}{}^*$. Furthermore, Fig. 16 arranges only the plastic strain increment satisfying associated flow rule, $d\varepsilon_{ij}{}^{p(AF)}$, in the same relation as Fig. 15. The component $d\varepsilon_{ij}{}^{p(AF)}$ is derived by removing the plastic component $d\varepsilon_{ij}{}^{p(IC)}$ and the elastic component $d\varepsilon_{ij}{}^{e}$ from the total plastic strain increment $d\varepsilon_{ij}$. Here, $d\varepsilon_{ij}{}^{p(IC)}$ and $d\varepsilon_{ij}{}^{e}$ are evaluated by Eqs. (21) and (44).

It is seen from Fig. 14 that the strain increment ratio $d\varepsilon_v/d\varepsilon_d$ depends not only on whether triaxial compression or extension condition but also on the kind of stress path. On the other hand, as is seen from Fig. 15, the strain increment ratio $d\varepsilon_{SMP}{}^*/d\gamma_{SMP}{}^*$ is almost independent of the difference between triaxial compression and extension near failure, whereas that is influenced by the kind of stress path except for near failure. It is also seen from Figs. 14 and 15 that the test results where mean stress increases(σ_3=const. and R=const.) deviate leftward and the test results where mean stress decreases (σ_1= const.) rightward from the dotted lines which denote the relation under constant mean stress (p=const.)in average. Now then, it is noticed that though the stress ratio-strain increment ratio relations in Figs. 14 and 15 are influenced by the stress condition and the stress path, the results in Fig. 16 are uniquely arranged.

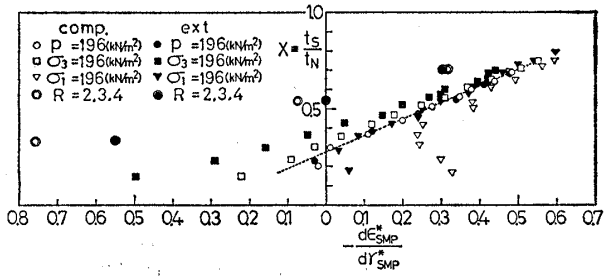

Fig. 15. Relation between t_S/t_N and $d\varepsilon_{SMP}{}^*/d\gamma_{SMP}{}^*$ in triaxial compression and extension tests under various stress paths

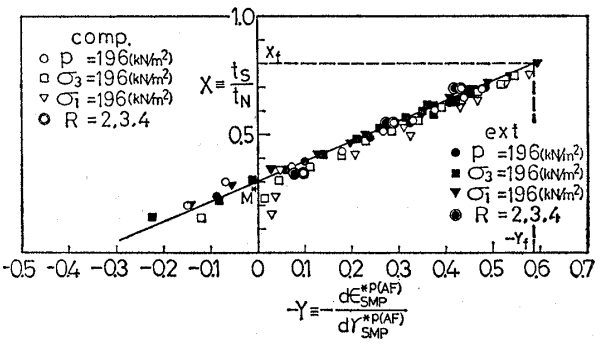

Fig. 16. Relation between t_S/t_N and $d\varepsilon_{SMP}{}^{*p(AF)}/d\gamma_{SMP}{}^{*p(AF)}$ in triaxial compression and extension tests under various stress paths

In Fig. 16, the relation of Eq. (23) (the linear solid line) calculated using the soil parameters mentioned before agrees well with the test results. Comparing these three figure, we can understand that introduction of the concept of t_{ij} is effective for describing uniquely the soil behavior in three-dimen sional stresses, and division of the plastic strain increment into two components

($d\varepsilon_{ij}^{p(AF)}$ of Eq. (16) and $d\varepsilon_{ij}^{p(IC)}$ of Eq. (17)) is effective for considering the influence of stress path on the soil behavior.

Analysis of Triaxial Compression and Extension Tests

Fig. 17 shows the observed values (dots) and the analytical curves of constant mean principal tests under triaxial compression and extension conditions, arranged in terms of the relation between principal stress ratio σ_1/σ_3 and principal strains (ε_1 and ε_3). The t_{ij}-sand model proposed here describes well not only the difference between compression and extension but also the tendency that the strains become large with increase in mean principal stress. Now, if we represent $d\varepsilon_v^e$ and $d\varepsilon_v^{p(IC)}$ not by a power law in Eqs. (19) and (20) but by linear relations between e and log p which are seen in clay, the calculated stress ratio-strains relation in these figures becomes to be independent of mean principal stress in the same way as t_{ij}-clay model.

Fig. 18 shows the obseved values (dots) and the analytical curves in various shear tests under triaxial compression and extension conditions in terms of the relation among σ_1/σ_3, ε_1 and ε_v. It is seen that t_{ij}-sand model describes the experimental results under various stress paths inclusive of the difference of soil dilatancy due to the stress path.

Fig. 19 shows the ε_v—log p relation in isotropic and anisotropic consolidation tests under triaxial compression and extension conditions. Here, the solid lines denote the analytical results and the dots the observed values, and R represents the principal stress ratio σ_1/σ_3. The analytical results describe the observed dilatancy under anisotropic con-

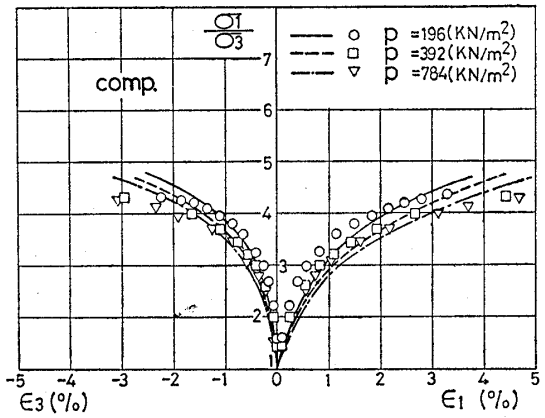

(a) triaxial compression

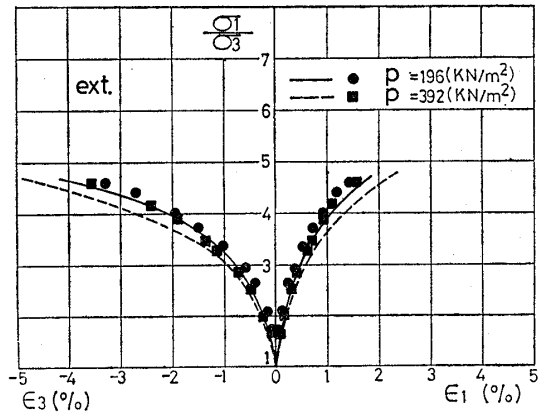

(b) triaxial extension

Fig. 17. Principal strains vs. principal stress ratio in constant mean principal stress tests

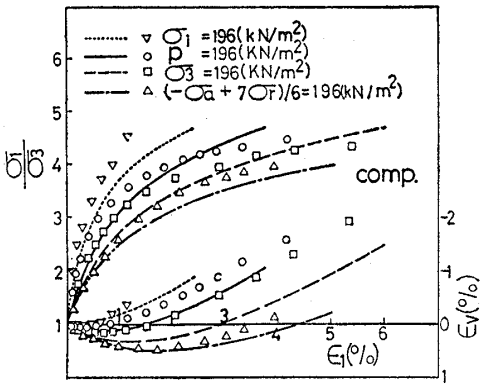

(a) triaxial compression

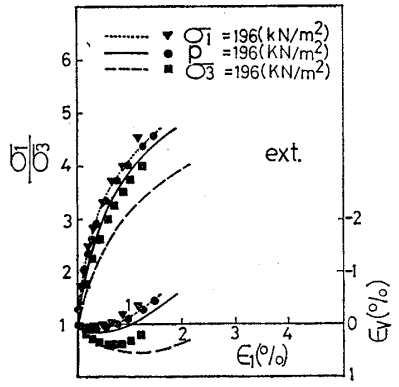

(b) triaxial extension

Fig. 18. Major principal strain vs. principal stress ratio and volumetric strain in various kinds of stress paths tests

solidation at high stress ratio, while it tends to overestimate. In figure (b), the observed volumetric strains of $R=4$ (▼) become less than those of R=1 but are still compressive. On the other hand, corresponding calculated result is expansive because of overestimation of dilatancy in particular. In Fig. 20 are arranged the results in shear tests ($p=196$ kN/m², 382 kN/m²) and consolidation tests ($R=1, 2, 3$ and 4), in terms of the relation between stress ratio σ_1/σ_3 and the strain

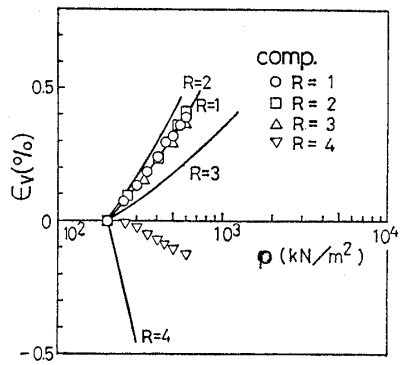

(a) triaxial compression

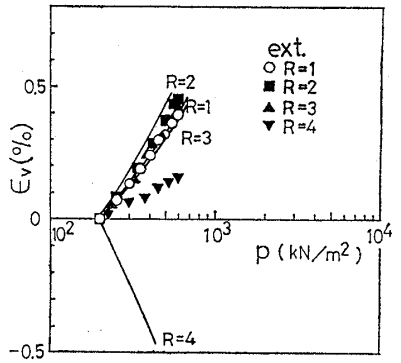

(b) triaxial extension

Fig. 19. Mean principal stress in logarithm scale vs. volumetric strain in isotropic and anisotropic consolidation tests

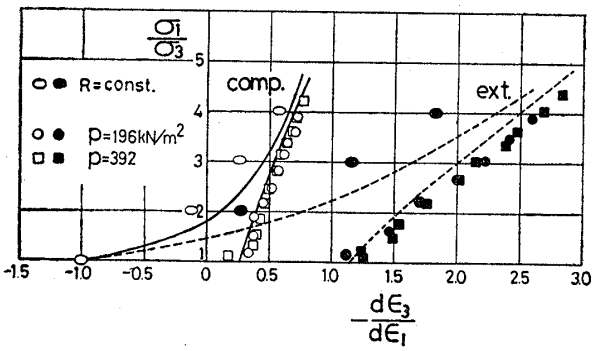

Fig. 20. Relation between principal stress ratio (σ_1/σ_3) and principal strain increment ratio ($-d\varepsilon_3/d\varepsilon_1$) in constant mean principal stress tests and constant principal stress ratio tests under triaxial compression and extension conditions

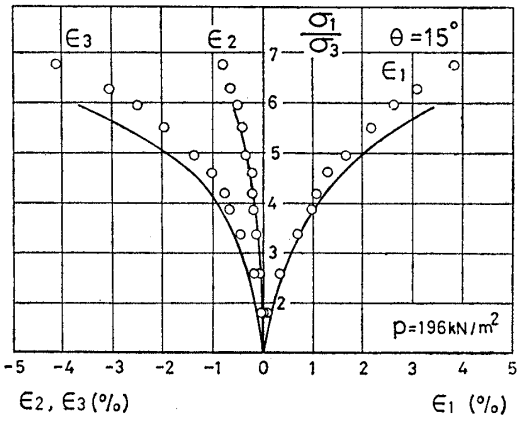

(a) $\theta=15°(b=0.268)$

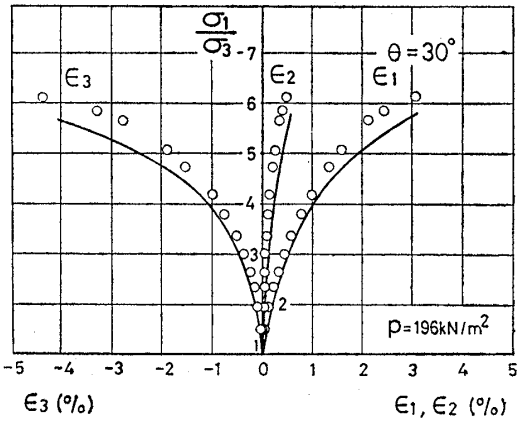

(b) $\theta=30°(b=0.5)$

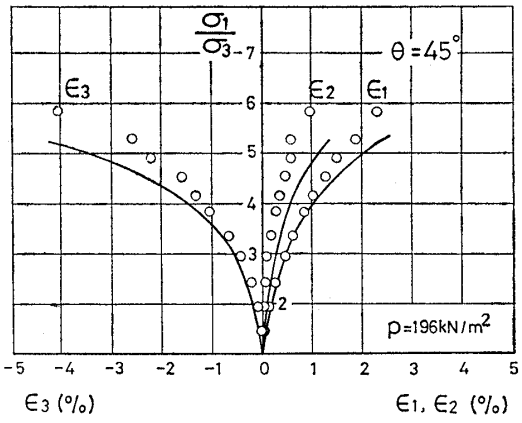

(c) $\theta=45°(b=0.732)$

Fig. 21. Principal strains vs. principal stress ratio in true triaxial tests under constant mean principal stress

increment ratio ($-d\varepsilon_3/d\varepsilon_1$). Here, open dots and solid lines represent the experimental and analytical results under triaxial compression condition, and solid dots and broken lines represent those under triaxial extension condition. Although there is a little difference between the experimental and analytical results in consolidation tests because of the overestimation of dilatancy mentioned above, the analytical results generally express the stress path dependency of strain increments in direction as well as the difference between triaxial compression and extension.

Analysis of True Triaxial Tests

Fig. 21 shows the observed values (dots) and the analytical curves of true triaxial tests under constant mean principal stress (p=196 kN/m²), arranged in terms of the relation between principal stress ratio σ_1/σ_3 and principal strains (ε_1, ε_2 and ε_3). Here, θ indicates the angle between σ_1-axis and the corresponding radial stress path on the octahedral plane—e. g. θ=0° and 60° represent the stress paths under triaxial compression and extension conditions, and $0°<\theta<60°$ the stress paths under three different principal stresses. Further, the parameter b which represents the relative magnitude of intermediate principal stress is defined as

$$b=\frac{\sigma_2-\sigma_3}{\sigma_1-\sigma_3} \qquad (50)$$

and is related to θ by the following equation :

$$b=\frac{2\tan\theta}{\sqrt{3}+\tan\theta} \qquad (51)$$

Figs. 22 and 23 show the observed and calculated directions of the strain increments on the octahedral plane in these tests, respec-

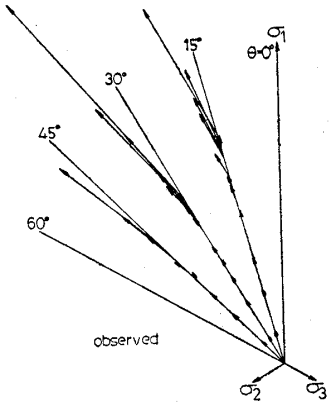

Fig. 22. Observed strain increment vectors on octahedral plane in true triaxial tests

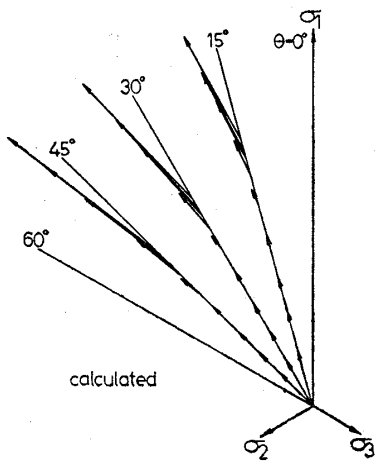

Fig. 23. Calculated strain increment vectors on octahedral plane in true triaxial tests

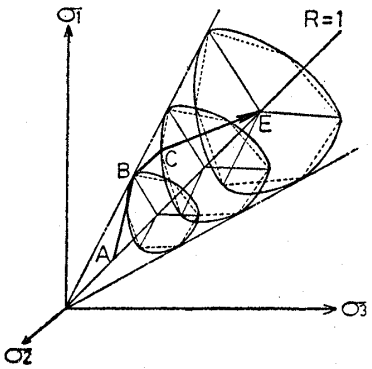

(a) path ABCE

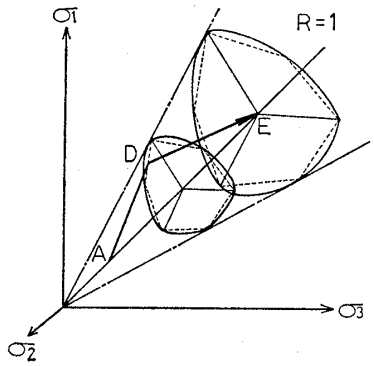

(b) path ADE

Fig. 24. Stress paths of true triaxial tests where values of b and p change

tively. The length of each vector is the amount of shear stain increment on the octahedral plane divided by the shear-normal stress ratio increment on the octahedral plane. As is seen from Figs. 21 to 23, the proposed model predicts well three-dimensional stress-strain behavior of sand, inclusive of the deviation of shear strain increment from shear stress in direction.

Next, let us analyze the true triaxial tests where the relative magnitude of intermediate principal stress and the mean principal stress change during shear loading. Fig. 24 shows the stress paths of tests in the principal stress space, together with the Mohr-Coulomb criterion represented by dotted curves and the SMP criterion represented by solid curves. The stress states in figures (a) and (b) change as follows :

(a) $A(\sigma_1=1,\ \sigma_2=1,\ \sigma_3=1)\rightarrow B(4,1,1)\rightarrow C(4,4,1)\rightarrow E(4,4,4)$

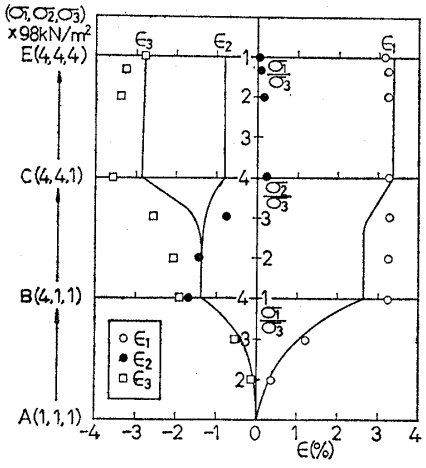

(a) path ABCE

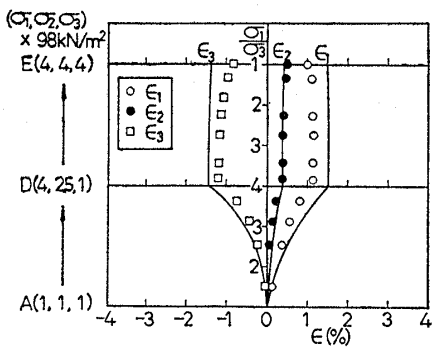

(b) path ADE

Fig. 25. Principal strains vs. principal stress ratio in true triaxial tests

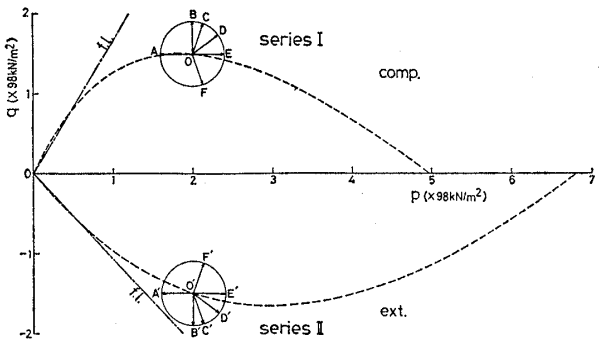

Fig. 26. Stress paths of stress probe tests (series I and II) represented in (p, q) space

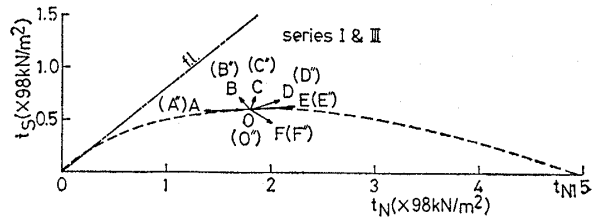

Fig. 27. Stress paths of stress probe tests (series I and III) represented in (t_N, t_S) space

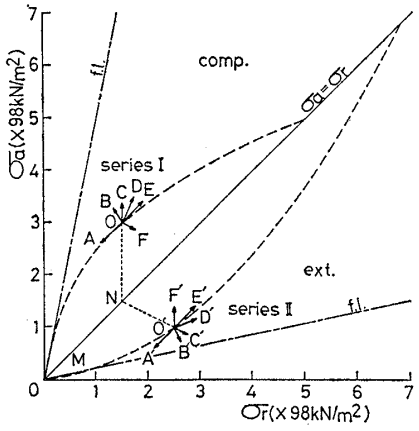

(a) series I and II

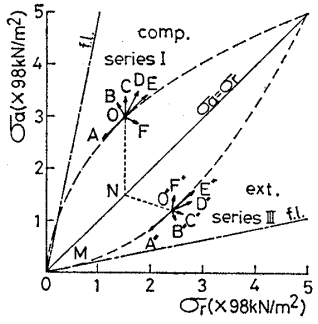

(b) series I and III

Fig. 28. Stress path of stress probe tests represented in (σ_a, σ_r) space

(b) A(σ_1=1, σ_2=1, σ_3=1)→D (4, 2.5, 1) →E(4, 4, 4)

where each unit of stress is ($\times$98 kN/m^2). Fig. 25 shows the observed values (dots) and the analytical curves under the stress paths in Fig. 24, arranged in terms of the relation between principal stress ratio and principal strains. It is seen from these figure that the proposed model describes the observed stress-strain behavior of sand under arbitrary three-dimensional stress path as well.

Analysis of Stress Probe Tests

As shown in Fig. 26, stress probe tests under triaxial compression condition (series I) are carried out by applying the stress increments (each magnitude is $\sqrt{(\Delta p)^2+(\Delta q)^2}$ =0.4) so that the stress state moves from the basic stress point O (p=2$\times$98 kN/m^2, q=1.5$\times$98 kN/m^2) to a corresponding point (A to F) respectively, with reference to the stress probe tests by Tatsuoka and Ishihara (1974). Further, two series of stress probe tests are carried out under triaxial extension condition. One is a series of tests (series II) whose stress paths are the same in (p, q) space as those of series I under triaxial compression condition (see Fig. 26). The other is a series of tests (series III) where the stress paths coincide with those of serises I in (t_N, t_S) space as shown in Fig. 27. The stress path vectors represented in (σ_a, σ_r) space of these three series are illustrated in Figs. 28 (a) and (b). In Figs. 26 to 28, the dash-dotted lines denote the failure lines and the broken lines the initial yield surfaces of t_{ij}-sand model.

Figs. 29 to 31 show the observed and predicted strain increment vectors in these three series of tests (left figures are the predicted and right figures the observed). Here, the volumetric strain increment $\Delta\varepsilon_v$ and the shear strain increment $\Delta\varepsilon_d$ are defined as $\Delta\varepsilon_v=\Delta\varepsilon_a+2\Delta\varepsilon_r$ and $\Delta\varepsilon_d=(2/3)(\Delta\varepsilon_a-\Delta\varepsilon_r)$ under triaxial conditions. From the comparison between the observed and predicted results in each figure, we can find that in general the model predicts well the variations in direction and magnitude of the

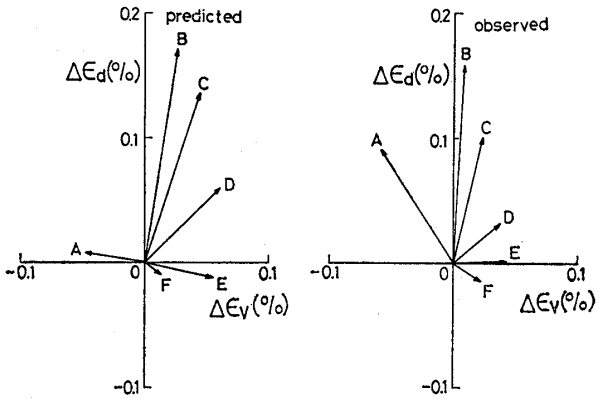

Fig. 29. Predicted and observed relation between $\Delta\varepsilon_d$ and $\Delta\varepsilon_v$ in stress probe test under triaxial compression (series I)

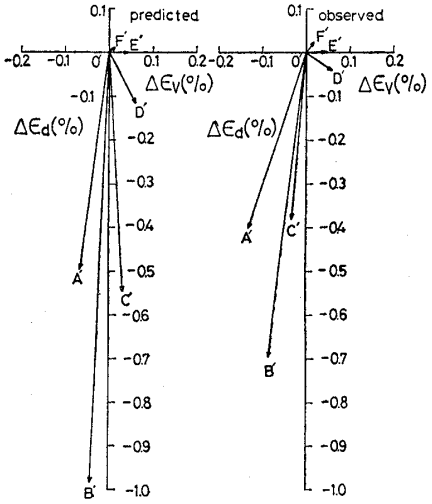

Fig. 30. Predicted and observed relation between $\Delta\varepsilon_d$ and $\Delta\varepsilon_v$ in stress probe test under triaxial extension (series II)

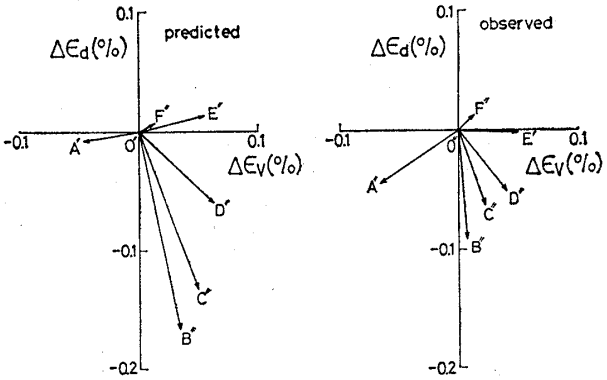

Fig. 31. Predicted and ovserved relation between $\Delta\varepsilon_d$ and $\Delta\varepsilon_v$ in stress probe test under triaxial extension (series III)

observed strain increment vectors due to the directions of stress probe. This is because the plastic strain increment is divided into two components ($d\varepsilon_{ij}^{p(AF)}$ and $d\varepsilon_{ij}^{p(IC)}$) in the model, though one yield function and one strain hardening parameter alone are used in the model.

Next, Let us compare the three series of tests each other. It is obvious from the comparison between Fig. 29 and Fig. 30 that there are large differences of the strain increments in direction and magnitude between triaxial compression and extension tests, though the stress paths of series I and II are the same in (p, q) space. On the other hand, the results of series III in Fig. 31 whose stress paths coincide with those of series I in (t_N, t_S) space almost correspond to the results where sign of $\Delta\varepsilon_d$ in Fig. 31 is inverted (since $\Delta\varepsilon_d$ is defined as $\Delta\varepsilon_d=(2/3)(\Delta\varepsilon_a-\Delta\varepsilon_r)$ in these figure), though in Fig. 31 the magnitude of observed vectors are a little small than that of predictd vectors. Therefore, it may also be noticed from the above comparison among three series that the three-dimensional stress-strain behavior of sand are uniquely described not by the model using (p and q) but by the model using (t_N and t_S) as the stress parameters.

CONCLUSIONS

The main results of this paper are summarized as follows :

(1) As a quantity of state for sand in three-dimensional stresses the "plastic work based on t_{ij}" W^{*p} is newly defined, and its validity is checked based on the experimental results.

(2) By employing W^{*p} as the strain hardening paramenter in place of the plastic volumetric strain ε_v^p in the model for clay, a simple and generalized elastoplastic model for sand (t_{ij}-sand model) is formulated. In the present model, the influence of the intermediate principal stress on the stress-strain behavior are considered by using the concept of t_{ij}, and the influence of stress path on the direction of plastic flow by dividing the plastic strain increment into two components regardless of a set of yield function and hardening parameter, in the same way as the t_{ij}-clay model proposed before. In addition, this model can describe both negative and positive dilatancies in three-dimensional stresses, unlike the model for clay.

(3) The model can predict well not only results of the triaxial compression and extension tests but also results of the true triaxial tests under various kinds of stress paths. The stress probe tests under triaxial compression and extension conditions can uniquely be analyzed by the model.

(4) It is also verified experimentally that the strain increment $d\varepsilon_{ij}$ is divided into three components (elastic strain increment $d\varepsilon_{ij}^e$, plastic strain increment satisfying associated flow rule in t_{ij}-space $d\varepsilon_{ij}^{p(AF)}$ and plastic strain increment compressive isotropically $d\varepsilon_{ij}^{p(IC)}$.

(5) All of the soil parameters of the model can be determined by a conventional triaxial compression test after loading-unloading-reloading isotropic consolidation.

ACKNOWLEDGMENTS

The author wishes to thank Prof. H. Matsuoka at Nagoya Institute of Technology for his continuing supports and useful discussions during the course of this study, and for his helpful suggestions on the way to use W^{*p} in particular. He is also indebted to Messrs. N. Hikita, N. Ebara, H. Takenaka, H. Shiomi, M. Takayanagi, K. Fujiwara, M. Horii and J. Fujii for their assistance with the experiments and the calculations.

REFERENCES

1) Henkel, D. J. (1960) : "The relationship between the effective stress and water content in saturated clay," Géotechnique, Vol. 10, pp. 41-54.

2) Matsuoka, H. and Nakai, T. (1974) : "Stress-deformation and strength characteristics of soil under three different principal stresses," Proc.,

JSCE, No. 232, pp. 59-70.
3) Matsuoka, H. and Nakai, T. (1977) : "Stress-strain relationship of soil based on the SMP," Proc., Specialty Session 9, 9th ICSMFE, Tokyo, pp. 153-162.
4) Nakai, T. (1987) : "Elastoplastic models considering the stress path dependency of soil behavior in three-dimensional stresses," Proc., 2nd Int. Conf. on Constitutive Laws for Engineering Materials ; Theory and Applications, Tucson, Vol. 1, pp. 429-436.
5) Nakai, T. and Matsuoka, H. (1983 a) : "Shear behaviors of sand and clay under three-dimensional stress condition," Soils and Foundations, Vol. 23, No. 2, pp. 26-42.
6) Nakai, T. and Matsuoka, H. (1983 b) : "Constitutive equation for soils based on the extended concept of "Spatial Mobilized plane" and its application to finite element analysis," Soils and Foundations, Vol. 23, No. 4, pp. 87-105.
7) Nakai, T. and Matsuoka, H. (1986): "A generalized elastoplastic constitutive model for clay in three-dimensional stresses," Soils and Foundations, Vol. 26, No. 3, pp. 81-98.
8) Nakai, T. and Mihara, Y. (1984) : "A new mechanical quantity for soils and its application to elastoplastic constitutive models," Soils and Foundations, Vol. 24, No. 2, pp. 82-94.
9) Roscoe, K. H. and Burland, J. B. (1968) : "On the generalized stress-strain behavior of wet clay," Engineering Plasticity, Cambridge Univ. Press, pp. 535-609.
10) Roscoe, K. H., Schofield, A. N. and Thurairajan, A. (1963) : "Yielding of clays in states wetter than critical," Géotechnique, Vol. 13, No. 3, pp. 211-240.
11) Schofield, A. N. and Wroth, C. P. (1968) : Critical State Soil Mechanics, McGraw-Hill, London.
12) Tatsuoka, F. (1972) : "A fundamental study on the deformation of a sand by triaxial tests," Dr. Thesis, University of Tokyo (in Japanese).
13) Tatsuoka, F. and Ishihara, K. (1974) : "Yielding of sand in triaxial compression," Soils and Foundations, Vol. 14, No. 2, pp. 63-76.

APPENDIX I

Concrete Expression of a_{ij} :

From Cayley-Hamilton's theorem, we have following equation

$$r_{ik}r_{kl}r_{ij}-I_1\cdot r_{ik}r_{kj}+I_2\cdot r_{ij}-I_3\cdot\delta_{ij}=0 \quad (A\,1)$$

where r_{ij} and δ_{ij} are a symmetric tensor and the unit tensor respectively, and I_1, I_2 and I_3 are the first, second and third invariants of r_{ij}. If we consider r_{ij} to be the stress tensor σ_{ij} to the one-half power such as

$$r_{ik}r_{kj}=\sigma_{ij} \quad (A\,2)$$

Eq. (A 1) becoms

$$r_{ij}(\sigma_{jk}+I_2\cdot\delta_{jk})=I_1\cdot\sigma_{ik}+I_3\cdot\delta_{ik}$$

Thus

$$r_{ij}=(I_1\cdot\sigma_{ik}+I_3\cdot\delta_{ik})(\sigma_{kj}+I_2\cdot\delta_{kj})^{-1} \quad (A\,3)$$

From Eq. (6), a_{ij} is expressed as

$$a_{ij}=\sqrt{J_3/J_2}\cdot r_{ij}^{-1} \quad (A\,4)$$

where J_2 and J_3 are the second and third stress invariants of Eq. (5). Substituting Eq. (A 3) into Eq. (A 4) gives

$$a_{ij}=\sqrt{J_3/J_2}\cdot(\sigma_{ik}+I_2\cdot\delta_{ik})\times(I_1\cdot\sigma_{kj}+I_3\cdot\delta_{kj})^{-1} \quad (8)$$

APPENDIX II

Verification of Eqs. (13) and (29) :

As is seen from Figs. 2 and 3, the second equal sign in Eq. (13) and the first equal sign in Eq. (29) are valid when $\overrightarrow{d\gamma_{SMP}{}^{*p}}$ ($\overrightarrow{NP}$ in Fig. 3) agrees with $\vec{t}_s$ ($\overrightarrow{NT}$ in Fig. 2) in direction. Since this agreement is necessarily shown under triaxial compression and extension conditions, let us check here the agreement under three different principal stresses.

Fig. A 1 shows the observed angle β be-

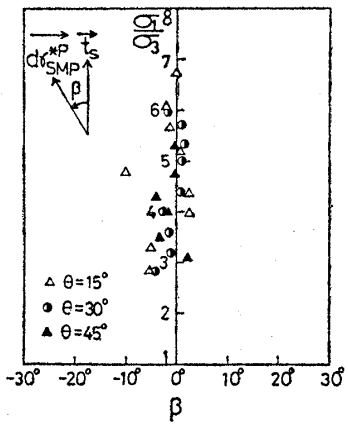

Fig. A 1. Principal stress ratio vs. angle between $\overrightarrow{d\gamma_{SMP}{}^{*p}}$ and $\vec{t}_S$ in true triaxial tests

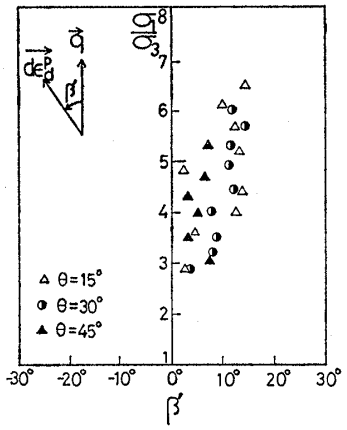

Fig. A 2. Principal stress ratio vs. angle between $\overrightarrow{d\varepsilon_d{}^p}$ and $\overrightarrow{q}$ in true triaxial tests

tween $\overrightarrow{d\gamma_{SMP}{}^{*P}}$ and $\overrightarrow{t_s}$ in the same true triaxial tests as those shown in Figs. 21 to 23. Since the observed angle β is almost zero degree regardless of the stress ratio and the stress path, we can see that Eqs. (13) and (29) are valid.

On the other hand, Fig. A 2 shows the observed angle β' between $\overrightarrow{d\varepsilon_d{}^p}$ and $\overrightarrow{q}$ in the same tests, on the basis of Mises' type parameters used in models such as Cam-clay model. Here, β' also indicates the angle between plastic shear strain increment $\overrightarrow{d\gamma_{oct}{}^p}$ and shear stress $\overrightarrow{\tau_{oct}}$ on the octahedral plane. It is seen that under three different principal stresses the angle β' is not zero degree and increases with the increase in stress ratio (it is also obvious from Fig. 22). Therefore, the following formulation is not valid except for under triaxial compression and extension conditions :

$$dW^p = \sigma_{ij} d\varepsilon_{ij}{}^p = p \cdot d\varepsilon_v{}^p + q \cdot d\varepsilon_d{}^p \qquad \text{(A 5)}$$

which is often utilized in most of models.